Geology, Geophysics & Environment 2020, vol. 46 (3): 205–222

The geomorphology of the Makran Trench in the context of the geological and geophysical settings of the Arabian Sea

Polina Lemenkova

Analytical Center; Moscow, 115035, Russian Federation; e-mail: pauline.lemenkova@gmail.com; ORCID ID: 0000-0002-5759-1089

Received: 10 June 2020; accepted: 1 October 2020; first published online: 27 October 2020

Abstract: The study focuses on the Makran Trench in the Arabian Sea basin, in the north Indian Ocean. The area is tectonically active, with a system of ridges and fracture zones morphologically separating the Arabian Sea. The study examined the relationships between the topographic structure of the Makran Trench and the regional settings of the Arabian Sea: geomorphology, sediment thickness, geophysical fields, geology and tectonic lineaments. The methodology is based on the GMT scripting toolset. The spatial analysis includes high-resolution datasets GEBCO, EGM2008, GlobSed and data on tectonics, geology, geophysics, sediment thickness and topographic terrain model visualized by GMT. The paper also defined a way in which the proprietary ESRI data format can be transformed into the freely available GMT geospatial data of the geoid EGM2008 model. The geomorphological modeling included the automatic digitization of 300-km width cross-section profiles of the trench demonstrating its submarine relief. The analysis showed a correlation between the geological and tectonic structures, asymmetric geomorphology and geophysical anomaly fields. Gravity data indicate a crustal structure with anomalies generated by the bending of the lithosphere into the Makran subduction zone and density variations in the mantle reflected on the gravity maps. The gravity correlates with lineaments of the geomorphic structures. Bathymetric analysis revealed the most frequent depth (448 samples) at –3,250 to –3,500 m, followed by intervals: –3,000 to –3,250 m, –2,750 to –3,000 m. The declining continental slope correlates with gradually decreasing depths as equally distributed bins: 124 samples (–2,500 to –2,750 m), 96 (–2,250 to –2,500 m), 86 (–2,000 to –2,250 m). The trench is an asymmetric form with a high steepness on the continental slope of Pakistan and low steepness with a flat valley on the oceanward side. The multi-source data integration is important for seafloor mapping and the geomorphological analysis of oceanic trenches hidden to direct observations. The machine learning methods of GMT and cartographic modeling provide possibilities for the effective visualization of the trench. The comparison of the geomorphology with gravity anomalies, tectonic lineation, geological structures and topographical variations provides more detail to studies of the seafloor in the Arabian Sea.

Keywords: geology, geophysics, cartography, GMT, Indian Ocean, Arabian Sea, Makran Trench

INTRODUCTION

The presented research focuses on the Arabian Sea and the Makran Trench located in its northern part (Fig. 1). The study is aimed at demonstrating a correlation between the seafloor structure of the submarine relief and its region settings: the geological and geophysical framework formed in course of its tectonic evolution. Although a deep-sea trench cannot be observed directly, its geomorphology can nevertheless be visualized via modelling and digital mapping. Most of the features forming a plate subduction zone can be detailed through comparative analysis, with high

resolution grids showing geophysical, topographical and geological data. The diversity of local geomorphic forms is consistent with both the heterogeneity of the Earth's crust and the high number of anomalies in the geophysical fields, which indicates tectonic disturbances, and the shape and location of the individual crustal blocks. Thus, submarine relief corresponds to a certain type of crust with a specific spectrum of the anomalous geophysical fields caused by rock density.

Besides a geomorphic response to the geophysical parameters and processes of plate tectonics reflecting movements of the Earth's crust, there is a certain correlation between climate conditions, e.g. glacier melt influencing sedimentation processes (Kuhn et al. 2006). Increased sediment transport contributes to relief changes by filling the trench axis. Sediment supply is largely controlled by the climate of the coastal land and weathering, together with the drainage and transport system to the sea. An example of a sediment flooded trench is Cascadia (west Canada), while an example of sediment starved trench is the Peru-Chile Trench (South America). The objective of this paper is to perform a geomorphological analysis of the Makran Trench in the context of the regional settings of the Arabian Sea, which is based on the GMT-based processing of high-resolution thematic data and modeling cross-section profiles of the trench. Data pool covering the region of the Arabian Sea consists of datasets including geophysical, geological, tectonic, topographic and gravity raster grids. The precision of both terrestrial and marine datasets such as GEBCO, EGM96, GlobSed provides an updated view of the regional conditions where the geomorphic structure of the Makran Trench was formed.

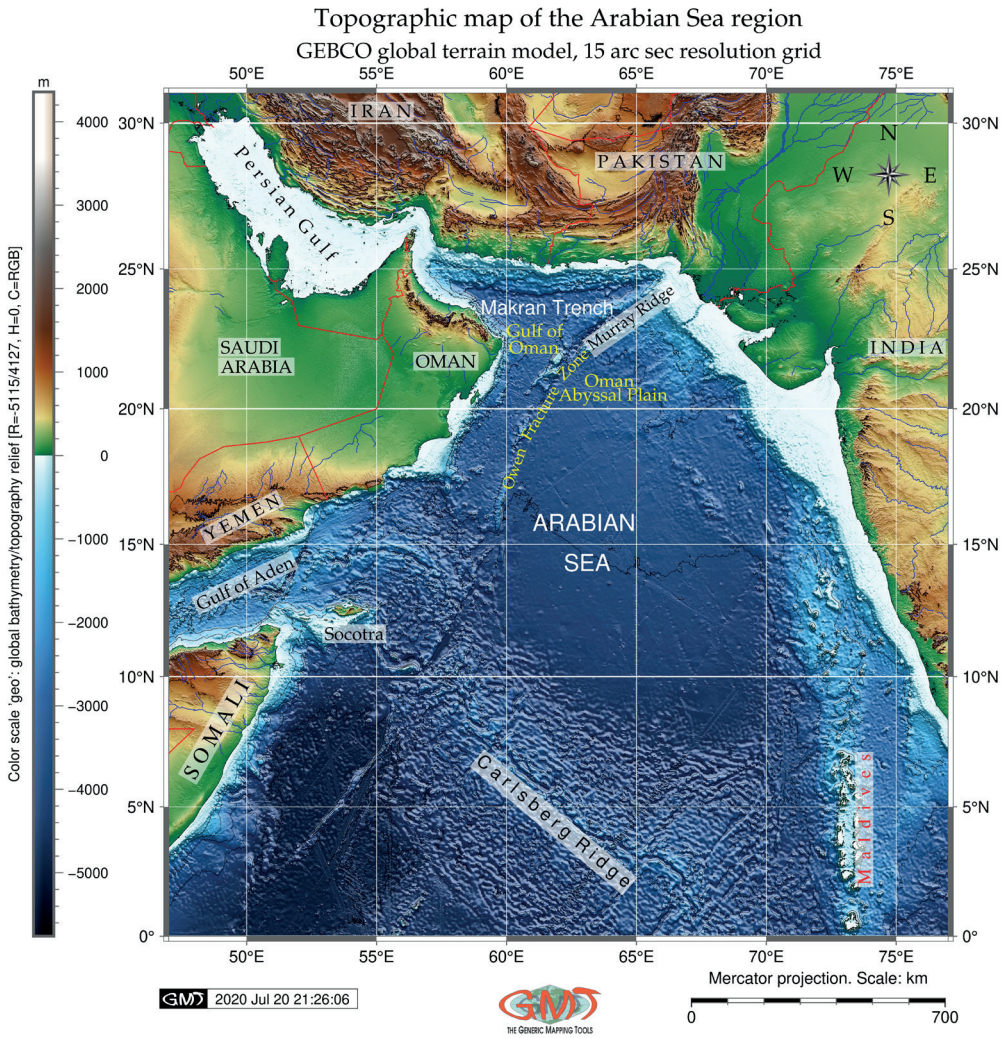

Fig. 1. *Topographical map of the Arabian Sea basin*

REGIONAL SETTING

Tectonics

The Makran Trench is formed in the subduction zone of the Arabian and Eurasian plates at the basement of the continental margin of Pakistan, in the zone of northward subduction of the high-velocity Arabian Plate beneath the continental crust of the low-velocity Eurasian Plate (Al-Lazki et al. 2014), Lut and the Afghan rigid block microplates (Abedi & Bahroudi 2016). The recorded convergence rate varies from ~4 cm/yr (Kopp et al. 2000) and ~2 cm/yr at the Gulf of Oman (Vernant et al. 2004). The subduction began during the Cretaceous period and is ongoing, forming an active trench-arc system and a seismic risk belt (Jacob & Quittmeyer 1979, Berberian et al. 1982, Laane & Chen 1989, Hussain et al. 2002). The subduction zone stretches along the NE margin of the Gulf of Oman, adjacent to the SW coast of Pakistan and the SE coast of Iran, Zagros Mountains (Paul et al. 2010, Regard et al. 2010). The geometry of the Makran subduction zone has a shallow angle with a slab deepening northward. The dip-angle of the slab is shallower under Pakistan in the eastern segment of Makran Trench (Farah et al. 1984). This might be caused by the differences in the subduction velocities in various regions of the subduction zone, as mentioned above.

The Zagros Mountains extend from the Turkish-Iranian border to the NW to the Makran subduction zone in the SE (Takin 1972). The Zagros Mts are one of the important tectonic units of the Alpine-Himalayan belt, formed on the NE edge of the subducting Arabian Plate, Persia-Tibet-Burma orogeny (Glennie et al. 1990). The topography of the Zagros Mts indicates the border of Late Cenozoic Tethys (Alavi 1980, Sengör et al. 1988). The Makran accretionary wedge arises adjusting the Makran Trench as a result of the accumulating sedimentary rocks of the Arabic Plate subducting into the mantle of the Eurasian Plate. The Makran accretionary wedge is one of the largest on Earth. It presents the belt of the Zagros collision system with the last remnants of the Neo-Tethys Ocean (Burg 2018). The spreading axis of Neo-Tethys inverted at 100–95 Ma absorbed in the subduction zone, built by the crust of the Arabian Plate colliding with Eurasian Plate below the Oman Abyssal Plain (Delaloye & Desmons 1980, Schlüter et al. 2002). The Makran accretionary wedge is marked by strong deformation of the sedimentary material destroyed by numerous thrusts (Grando & McClay 2007).

Geology

The geological setting of the Makran region of the Arabian Sea formed as a result of the tectonic processes briefly described above and more detailed in the existing studies (Kananian et al. 2001, Haghipour et al. 2015, Motaghi et al. 2020). Particularly notable are the system of ridges and fracture zones which separate the Arabian Sea into morphologically distinct basins (Fig. 2). The northwestern branch of the ternary system of Mid-Indian Ridge consists of several parts. From the triple joint, it stretches in a direction close to the meridional and then continues from the region of 3°N and 67°E in the NW direction as the Carlsberg Ridge, a slow-spreading ridge with rate of 26 mm/yr (Murton & Rona 2015). The Makran subduction zone has shallow seismicity with frequent moderate-level earthquakes.

However, the seismicity differs in the eastern and western parts of the region, with a rough boundary between the two zones at ca 62°E (the border between Iran and Pakistan). The seismicity is low in its western segment and high in the east, where large-magnitude frequent earthquakes are recorded. Such spatial difference might be caused by a segmentation of the subduction zone (Rani et al. 2011). The region also has high hydrocarbon potential (Harms et al. 1984).

The horizontal movements of the Arabian Plate have repeated during the geological evolution of the region with the main geological structures formed by the end of Miocene. Some residual shallow inland seas persisted inland of the Makran through the Neogene (McCall 1997). The Owen Fracture Zone marks the area where the old oceanic lithosphere was rifted to form the Sheba Ridge (Stein & Cochran 1985). The system of these rift complexes was formed in Miocene during the opening of the Gulf of Aden, from the Gulf of Aden to the African-Antarctic Range in the SW of the Indian Ocean (Hunziker et al. 2015).

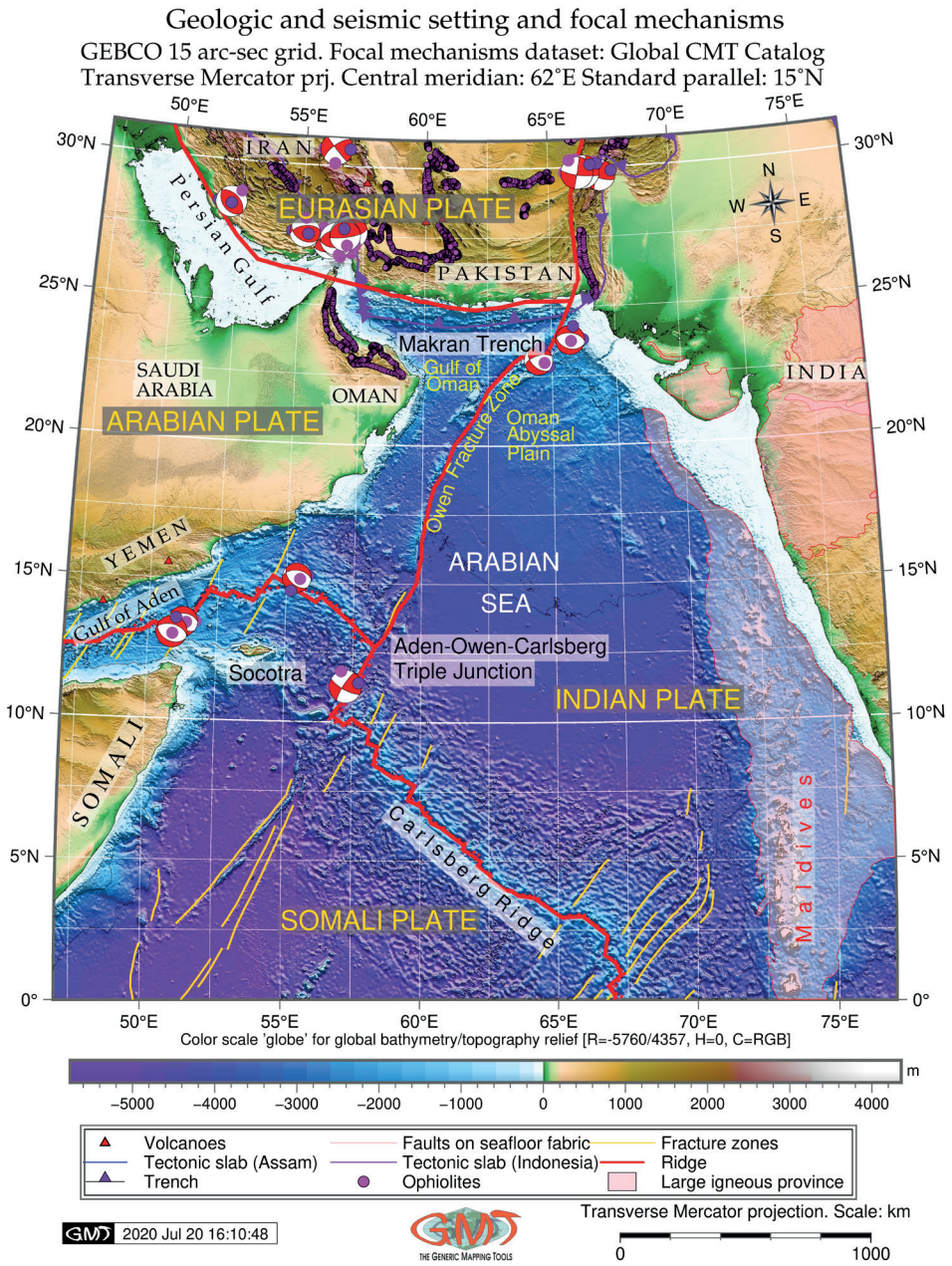

Fig. 2. *Geological and seismic map of the Arabian Sea basin*

The NW Arabian Sea and the Indian plate margin are characterized by several phases of volcanism and deformation (Gaedicke et al. 2002). Ridge inversion resulted in intra-oceanic subduction with an arc magmatism producing the lavas covering Oman ophiolite, the largest piece of oceanic crust exposed on land (Goodenough et al. 2014). The ophiolites formed submarine elevations in the Late Cretaceous–Eocene period until the Early Oligocene (Burg et al. 2013). The Oman ophiolites are remnants of the ancient oceanic crust which have risen to the surface. Cretaceous active volcanism is indicated by the recorded heavy minerals and dioritic pebbles and turbidites of the Makran accretionary wedge.

Geomorphology

The Makran Trench stretches for 1,000 km along the northeastern margin of the Gulf of Oman, southeast of Iran and southwest of Pakistan. Geometrically, it has a slightly arcuate form and ca. 350 km width (Burg 2018). Topographically,

the Makran subduction zone is located in the northern part of the Arabian Sea (Fig. 1) where the seafloor is generally inclined to the south with depths increasing from 3,000 to 4,800 m. The geomorphic structure of the Arabian Sea seafloor is complicated by numerous faults and rifts, the Carlsberg Ridge, and the Owen Fracture Zone. The seafloor surface here is leveled and complicated by channels of suspension flows diverging from the mouth of the Indus (Fig. 1). The crustal block structure of the Murray Ridge reaches depths of –2,000 m (Minshull et al. 2015). The Murray Ridge and Owen Fracture Zone separate the local basin of the small Gulf of Oman with rather flat seafloor at depths of about –3,300 m. The western part of the Arabian Sea has a shallow shelf stretching along the coasts of the Arabian Peninsula, Iran and Pakistan, with depths below 80–100 m. The surface of the shelf along the coasts of Oman and Saudi Arabia is complicated by numerous coral reefs. The continental slope along the coast of Oman is presented by a ledge with valley-block dissections. The continental slope along the coasts of Iran and Pakistan has a step-block structure at depths of 3,000–3,400 m.

The Carlsberg Ridge is the most notable geomorphological structure in the Arabian Sea, discovered by the Danish R/V 'Dana' during the Carlsberg Foundation's Oceanographic Expedition in 1928–1930 (Wolff 1967). It is directed NW until the 10°N. At 10°N, the Carlsberg Ridge is dissected by the large transverse Owen Fracture Zone with a total length in the adjacent basins of 2,800 km, including Chain Ridge and Murray Ridge (Rodriguez et al. 2014). Then, it changes direction to almost 90° until 12.5°N before continuing as the Aden-Sheba Ridge in the Gulf of Aden (Fig. 2). The Carlsberg Ridge is characterized by the extended block-ridge geomorphic structures in the rift zone and on the flanks. Its geomorphology was affected by the northward drag of the Arabian Plate caused by the Indian Plate across the northern Owen Fracture Zone (Bosworth et al. 2005). The end of this rift system is a graben of the Gulf of Tadjoura, which is a direct continuation of the Aden-Sheba Ridge and the rift graben branching to the NW of the Red Sea through the Gulf of Aden. These grabens might be a form of rift intrusion within the continent.

The depths in the rift valleys exceed –3,500 m, in some places up to –4,200 m, and above the ridge mostly –2,300 to –2,800 m, with rare transverse faults located within the rift zone. The fracture zone within the mid-ocean ridge is presented by a system of alternating parallel ridges and gutter-shaped narrow elongated minor trenches. Here the depths exceed –4,000 m (maximal depth –5,803 m) ranging 2,500 to 3,500 m above the ridges. The largest submarine peak is the flat-headed Error Seamount (Mount Error Guyot), a shallow guyot located in the Arabian Sea with a minimal depth of 368 m, notable for its phosphorites, dense slabs and irregular lumps associated with limestones (Purnachandra Rao 1986). The displacement of the rift structures along the fault is 330 km.

Sedimentation

The interplay between the tectonics, climate change and melting of glaciers controls the input of terrigenous sediment along the active Makran convergent zone (Bourget et al. 2010). The conditions of sediment formation, storage rates, and capacity of transport from fluvial systems and nature of sediment supply correlated to the climate changes, sea-level, and lithosphere movements affecting source-to-sink sediment dispersal patterns. Climate controls the currents that feed the turbidite system. In turn, it controls the sand-to-mud ratio in the deep-water deposits in trench areas.

Active deformation of sediments at a compressive plate boundary causes the tectonic thickening of the sediment column (White & Klitgord 1976). These processes take place at the continental margin near the Makran Trench: sediments from the Oman Abyssal Plain are accreted in a series of folded sediment ridges parallel to the coast and gradually changing seafloor geomorphology. In turn, the thick sediment layer hides submarine geomorphic features, e.g. Laxmi Ridge, a large-scale basement high buried beneath the sediments of the Indus Fan (Bhattacharya et al. 1994, Miles et al. 1998). On the one hand, the transport, relocation and distribution of the sediments are caused by the movements of the Earth's crust, submarine relief and currents. On the other, sedimentation can be associated with climate change and in turn this affects the geomorphology of the seafloor through the accumulation and deposition processes.

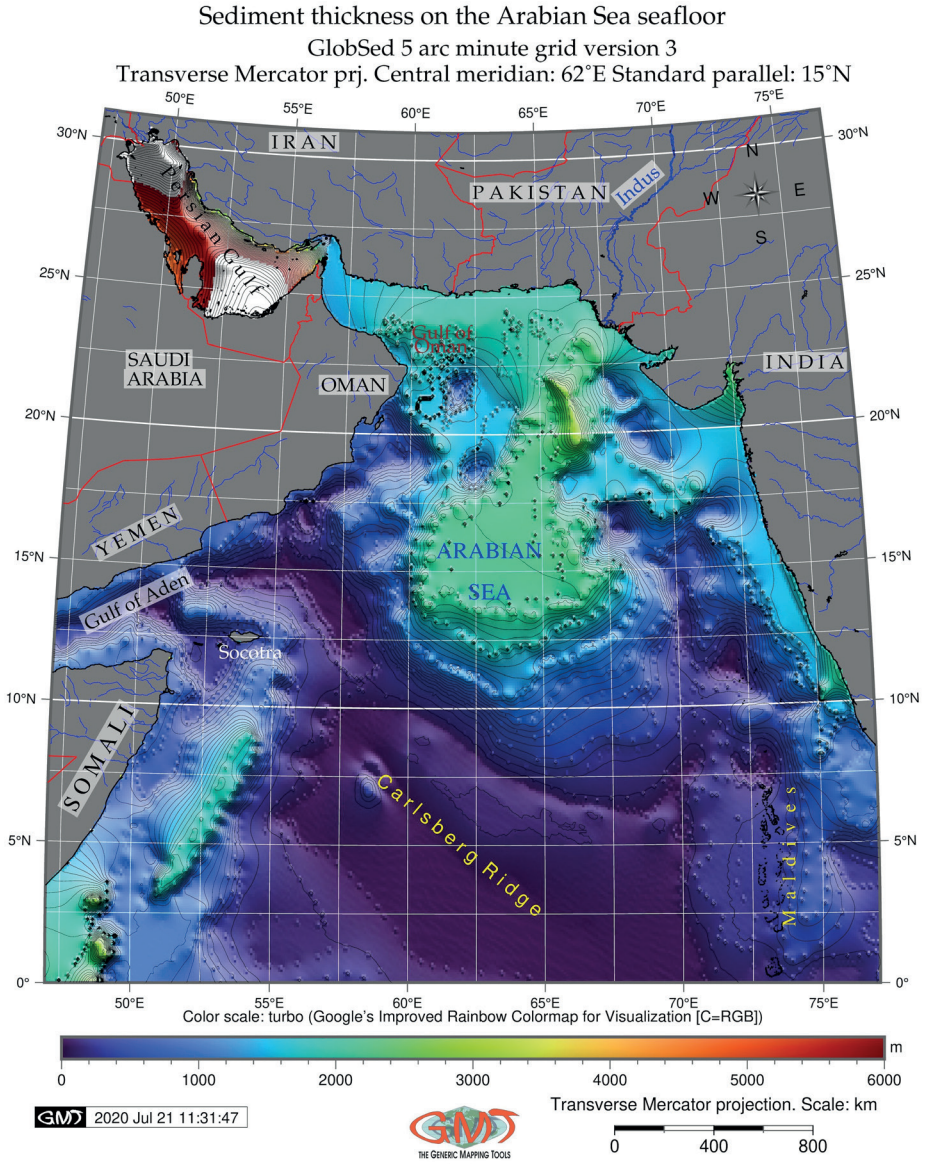

Fig. 3. *Sediment thickness of the Arabian Sea basin*

The sediment thickness of the Arabian Sea has an uneven distribution clearly distinct for its shelf northern areas and southern outer waters (Fig. 3). The sediment thickness is maximal (up to 2500–3000 m) in the northern part of the Arabian Sea, near the mouth of Indus River (runoff of 435 Mt/yr) and smaller rivers (Narmada, Tapti). Compared to the outer parts of the sea, the Makran subduction zone has a higher sediment input with a thickness of 7 km and a shallow subduction angle (Kopp et al. 2000, Smith et al. 2014). According to recent studies (Ellouz-Zimmermann et al. 2007), the sediment input in the Makran originated during Cenozoic from various sources: direct influx from the Indus River Valley, Indian shield and Himalayas, and the strong erosion of the growing Makran accretionary prism. The sediment thickness only decreases to less than 0.5 km in the pelagic zone of the Arabian Sea, reaching values typical for the open parts of the ocean (Neprochnov 1961). The width of the zone with higher values of the sediment thickness (0.5 to 2.5 km and more) is about 1.5 km (Lisitsyn 1974). The sedimentary material from the Indus River, along with carbonate, provides significant input to the Arabian Sea overcoming the Mid-Indian Ridge and entering the Somali Basin. More details on sedimentation of the Arabian Sea are provided in existing studies (White 1982,

Searle et al. 1983, Platt et al. 1985, Prins et al. 2000, Hosseini-Barzi & Talbot 2003).

Geophysics

Geophysical data provide an important indication of the Earth's crustal structure: the gravity anomaly is generated by the bending of the oceanic lithosphere into the Makran subduction zone and density variations in the mantle lithosphere. Mantle density variations (denser or thicker) reflected on the gravity maps are caused by the crustal structure in the areas of tectonic plate subduction and the effects of faults (Linsser 1967). Hence, tectonics can be investigated on the maps of gravity undulations. Example of such studies already exist (Awad et al. 2001, Selim & Aboud 2012). High-resolution marine free-air gravity maps across the Arabian Sea and Makran margin corroborate the difference in the crust gravity anomalies. The comparison of the gravity anomalies with lineations of the topographical structures permits more detailed seafloor spreading, and in particular, some of the basement features and geomorphic objects in the basin of the Arabian Sea. The Carlsberg Ridge which crosses the Arabian Sea is generally characterized by weakly positive marine free-air gravity anomalies 10 to 50 mGal (orange to red colors, Fig. 5).

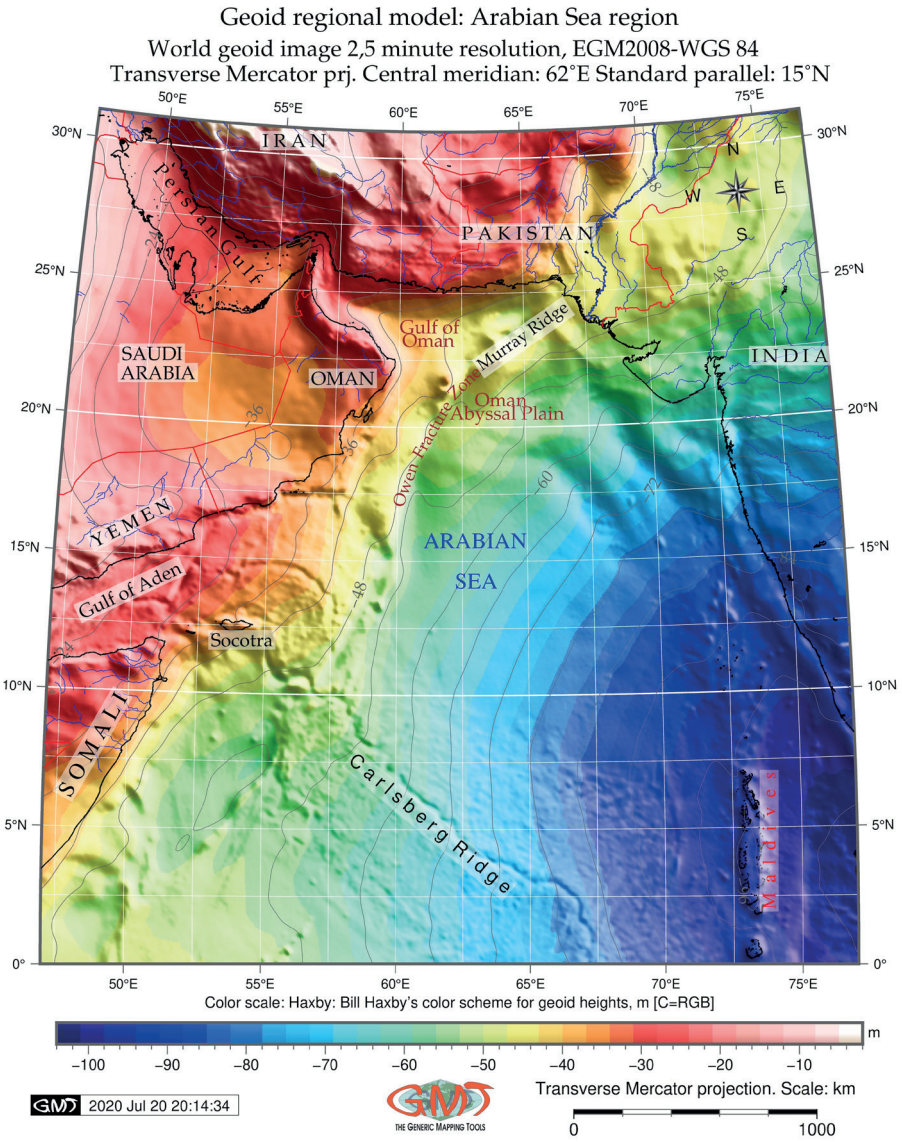

Fig. 4. *Geoid model of the Arabian Sea basin, based on the EGM2008 raster data set of 2.5-minute geoid undulation covering the Arabian Sea*

At the same time, the basin of the Arabian Sea is characterized by lower marine free-air gravity values: –20 to 5 mGal (light green to yellow colors, Fig. 5).

According to the visualized map (Fig. 5), there are strongly negative anomalies with an amplitude of –70 mGal and below (dark blue colors in Figure 5) in the Owen Fracture Zone, Murray Ridge and the Makran Trench. The transverse dimensions of the Carlsberg Ridge (20–40 km) corresponds to the size of the blocks composing the ridge submarine relief. In the rift zone above its western parts, the marine free-air gravity anomalies are positive, taking up to 40 mGal (red colors, Fig. 5), above its further flanks the anomalies become slightly negative (0 to –20 mGal), and above the rift valley a minimum of –60 mGal is noted (blue color depicting the valley of the Carlsberg Ridge). Local variations in the marine free-air gravity anomalies indicate the horizontal density heterogeneity of the Earth's crust and its block structure. Rock bodies causing gravity anomalies over the Carlsberg Ridge indicate that their upper layers are located on the seafloor surface, while lower ones are at depths of –10 to –15 km, i.e. on the border with the anomalous Earth's mantle. This may affect the distribution of gravity anomalies over the Arabian Sea seafloor.

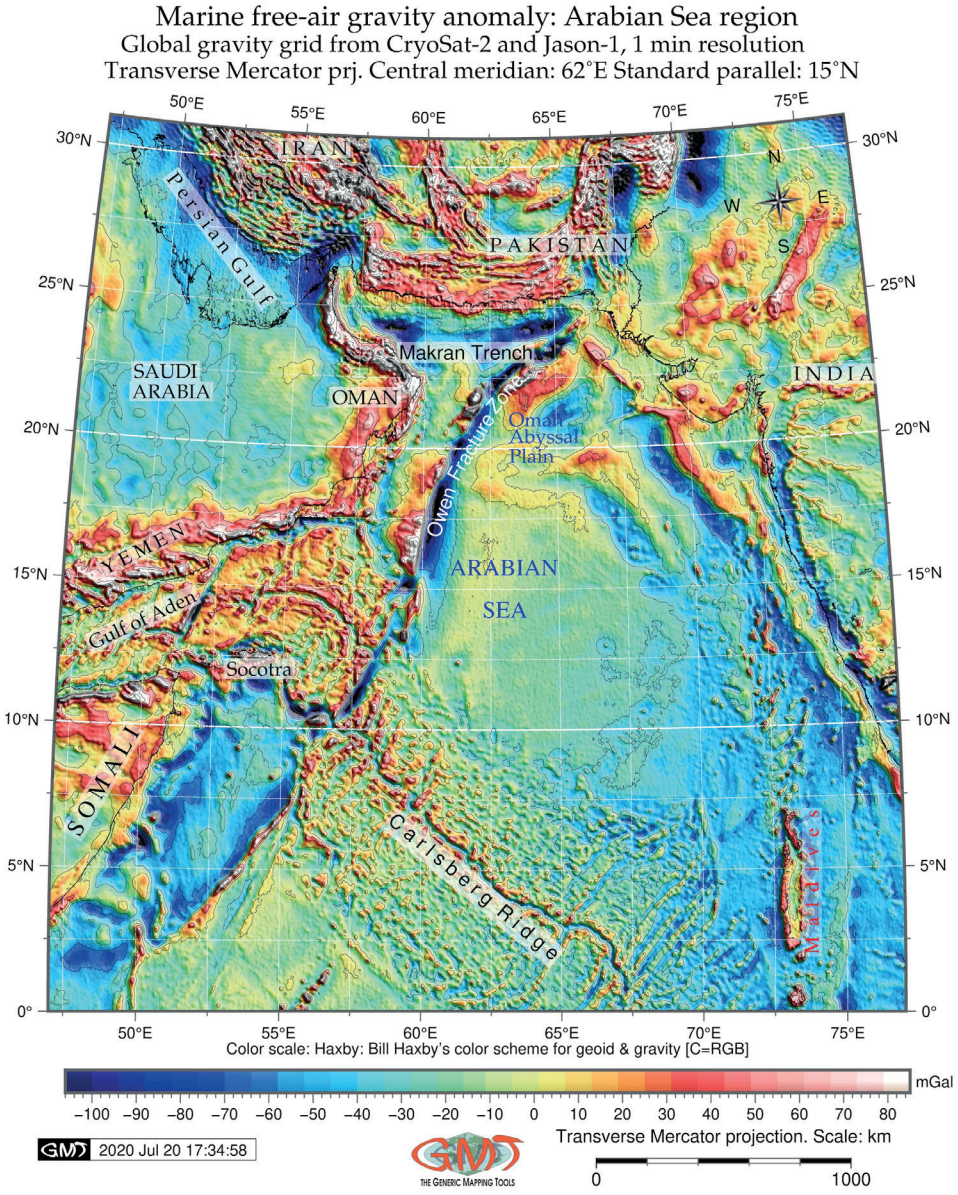

Fig. 5. *Marine free-air gravity map of the Arabian Sea basin*

MATERIAL AND METHODS

The technical methodology is based on the Generic Mapping Tools (GMT), a free open-source cartographic toolset (Wessel & Smith 1991, Wessel et al. 2013). The GMT was used for mapping, visualizing, data format converting and automated digitizing, plotting graphs of the cross-sectional profiles and modelling. The algorithms of GMT syntax and shell scripts are described (Wessel & Smith 2018, Lemenkova 2020a, 2020b). The general topographical map (Fig. 1) and digitizing cross-sectional profiles of the Makran Trench (Figs. 6, 7) were based on using General Bathymetric Chart of the Oceans (GEBCO), a 15-arc second high-resolution raster grid covering bathymetry and topography of the Earth (Monahan 2004). The visualization of the GEBCO dataset was made using a series of GMT modules by means of the scripting approach described in existing works (Lemenkova 2019g). Geological datasets were derived from the Scripps Institution of Oceanography datasets. Focal seismic mechanisms were plotted using dataset from the global CMT project (Ekström et al. 2012).

The geoid data was modeled using a raster grid based on EGM2008 (Fig. 4), a geopotential model of the Earth's gravity fields with a resolution of 2.5 minutes (Pavlis et al. 2012), which is an updated version of the previous EGM96 with a 15-minute resolution (Lemoine et al. 1998). A subset of the global 2.5 × 2.5-minute grid of the computed geoid undulation values of the EGM2008-WGS 84 was made using the conversion of the initial ESRI GRID to the GMT by a GMT command 'grdconvert cent2_geoid/ EGM2008ME.grd', which exchanges the initial ArcGIS raster format with an 'adf' extension into the GRID format (EGM2008ME.grd) readable by GMT. Here, the 'cent2_geoid/' is a folder with an ESRI grid. The space indicates the grid file has been compiled from the ESRI format (w001001.adf).

The file was visualized by the GMT codes 'ps=Geoid_EGM2008.ps' and 'gmt grdimage EGM2008ME.grd -Ccolors.cpt -R20/90/-5/60 -JM6i -P -I+a15+ne0.75 -Xc -K > $ps'. Since the ArcGIS ESRI GRID rasters are stored in a folder, it contains an 'Info' subfolder and auxiliary file (with an AUX extension) and a subfolder with seven technical files that store metadata (.xml), geographic coordinates, header information (prj.adf, hdr.adf, sta.adf, dblbnd.adf) and the actual raster data for the corresponding grid. This GRID format represents a continuous surface of geoid undulation where each cell derives the value from the original computed geoid undulation value located at the SW corner of each cell (Pavlis et al. 2012).

The free-air gravity map was used to depict the broad tectonic and topographical characteristics (Smith & Sandwell 1997). The dataset for global free-air marine gravity was received from the available grids modeled by the remote sensing survey from CryoSat-2, Jason-1 retrieved from Scripps Institution of Oceanography (Sandwell et al. 2014). Mapping marine free-air gravity is essential in a variety geological applications, such as determining structures of crust, quantitative assessments in resource exploration, metallic ores, near-surface voids, determining subsurface and salt structures, defining depths of the crystalline basement complex, computing changes of fluid or gas content in volcanoes (Hinze et al. 2013). In general, the interpretation of the marine free-air gravity anomalies correlates with values of the approximate bathymetric depths and the density of known geological or geophysical datasets. The original dataset in GRID format presents the pre-computed gravity response of the rock structure calculated with a modeling algorithm (Sandwell et al. 2014). The technical details of mapping free-air gravity by GMT were derived from Lemenkova (2020c).

The sediment thickness was modeled using a GlobSed raster grid, Version 3, with a computed total sediment thickness of the Earth's oceans and marginal seas (Straume et al. 2019). A sediment thickness grid was compiled based on the 5-minute resolution data grid from NOAA, the World Data Service for Geophysics, received by the seismic reflection and refraction data and compiled for the world areas. The sediment thickness enables the identification of the variability of the sediment deposition along the Arabian Sea, Makran and western margins of Hindustan, which demonstrates a correlation with Indus river discharge. The sediment grid depicts lower values distributed relatively evenly in the outer (southern) margins

of the Arabian Sea and generally higher values near the coastal zones. The values change markedly in the Persian Gulf where the values exceed the 5,000 m. the area of the Makran Trench has dominating values between the 1,800 to 2,600 m. By mapping the GlobSed grid, the regions of the sediment deposition can be identified, which suggests various sediment sources: pelagic, hemipelagic, alluvial and glacial drainage outlets from the continent (mainly, the Indus River and minor rivers in the study area).

Geomorphological slopes of the Makran Trench were identified and visualized from a gridded bathymetry data set (GEBCO 15 arc-second grid), which is based on the satellite-derived gravity-predicted depths (Mayer et al. 2018). The cross sectional profiles, each with a 300-km length, were drawn using a combination of the GMT modules 'grdtrack', 'convert' and 'psxy' and a Unix utility 'cat' using an existing technology (Lemenkova 2019b, Lemenkova 2019c) across the segments with coordinates 61.3°E 24.1°N (1st point of the segment) to 63.7°E 24.2°N (2nd point of the segment) (Fig. 6B). The cross-sections are visualized in Figure 6. The red line connected by two points means a target segment with start and end points at coordinates 61.3°E 24.1°N to 63.7°E 24.2°N (Fig. 6B).

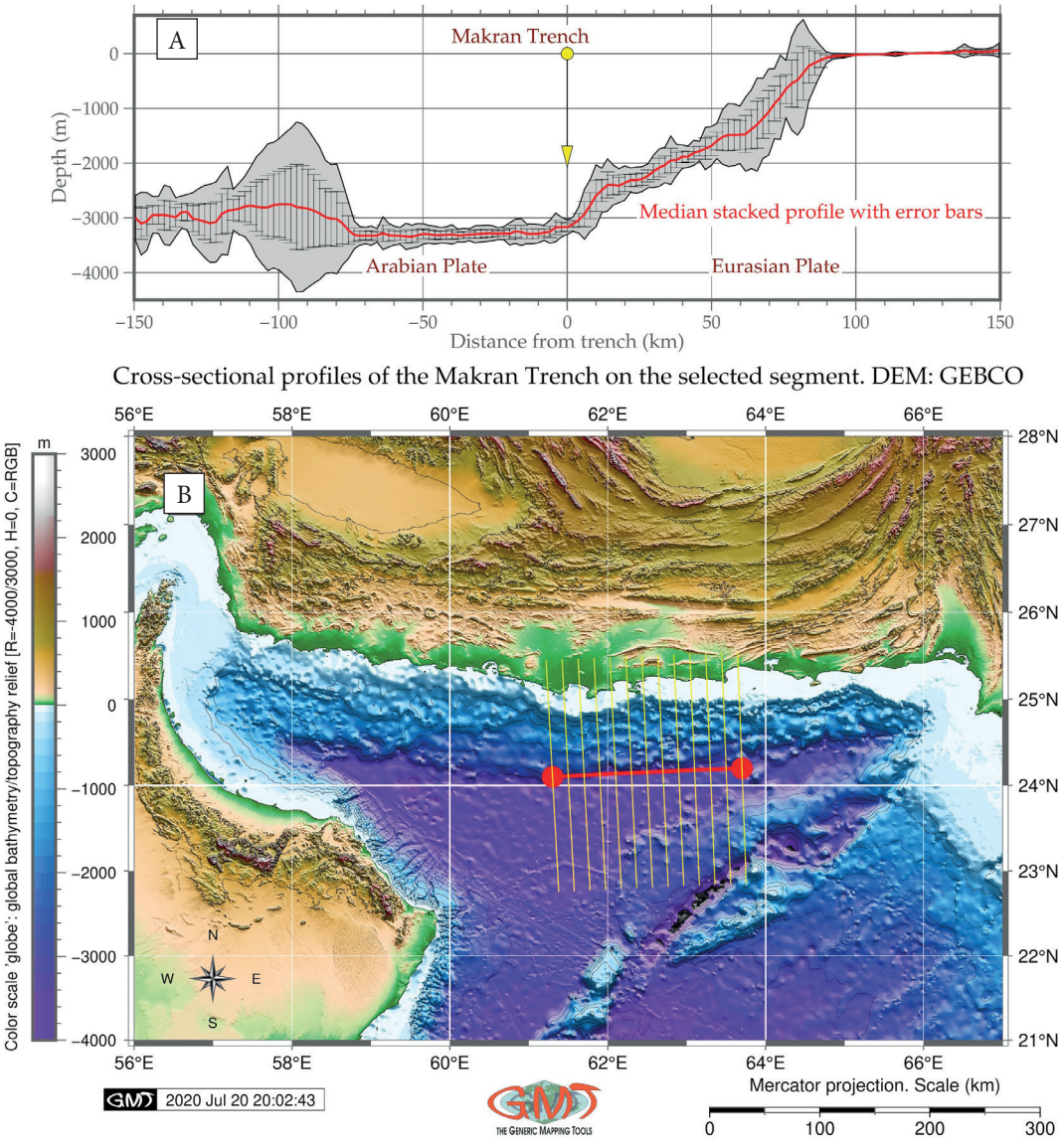

Fig. 6. *Makran Trench: cross-section profiles and graph*

The perpendicular sections mean 13 cross-section transects. The length of each cross-section is 300 km. The profiles were spaced at 20 km (the distance between every two cross-sections, yellow thin lines in Figure 6B) and sampled every 2 km (that means, the depth point was measured every 2 km along the 300-km line of each cross-section). The cross-sections are shown as flanks with a trench axis at 0 and 150 km at both flanks (Fig. 6A): the graph of the profile runs at X axis from –150 to 150 passing 0 where the trench axis is located. Technically, the cross-sections were plotted in a GMT script by the 'grdtrack' module using the following code: 'gmt grdtrack trenchMAK.txt -Gmak_relief.nc -C300k/2k/20k+v -Sm+sstackMAK.txt > tableMAK.txt' and 'gmt psxy -R -J -W0.5p, yellow tableMAK.txt -O -K >> $ps'. Figure 6A shows the median of the cross-section profiles as red line. The cross-sections are crossing the Makran Trench in a perpendicular direction (as indicated in Figure 6A). Accordingly, the bathymetric depths vary within each of the segment as shown on the histogram (Fig. 7). From each profile, the statistics on the Makran Trench depth (minimum, maximum, median, and a standard deviation) were recorded and visualized over the range of –4,000 to 1,000 km. A rose diagram shows the distribution of the topographical slope directions (Fig. 7) by modules 'pshistogram', 'psrose' and 'pslegend' for plotting (Fig. 7).

RESULTS

The symmetry of the ocean floor structure is demonstrated as a visualized distribution of the gravity anomalies, geological formation, geoid and topographical terrain (Figs. 1–5). Clearly discernible rift anomalies associated with the formation of a new oceanic crust and with the uplift of the deep matter stretch along the axis of the Makran Trench, Carlsberg Ridge and Owen Fracture Zone. On both sides of these geomorphic structures, the anomalies are symmetrically distributed, correlating quite well with local structural forms of the submarine relief.

Fracture zones and numerous transform faults are clearly visible along the stretching directions of the marine free-air gravity anomalies, dissecting the Carlsberg Ridge and in some cases entering ocean basins (comparing Figures 1, 2 and 5). Sediment thickness clearly correlates with the Indus River mouth and inflow (Fig. 3) dividing the Arabian Sea into the two regions that in turn correlate with the valley of the Carlsberg Ridge serving as a natural border (compare Figures 2 and 3). The geoid regional gravitation model (Fig. 2) clearly shows the division of the Arabian Sea basin roughly diagonally into two regions according to the values of the undulations: NW area: slightly negative values from 0 to –45 (red, orange to yellow colors in Figure 4) and strongly negative values from –45 to over –100 (yellow, green to blue colors in Figure 4) with the most negative anomalies around the Maldives (Fig. 1).

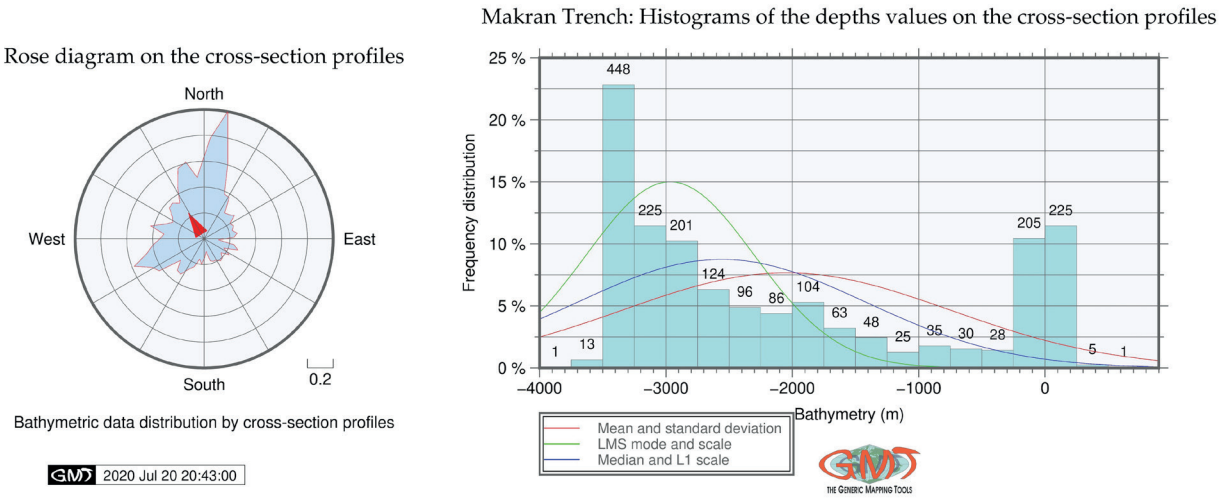

Fig. 7. *Makran Trench: statistical histograms of the cross-section profiles*

The gravity model demonstrates the responses of the geophysical structure to the variations in lithology and inferred depths realized from the satellite-derived gravity data (Fig. 5). The gravity field gives an integrated response to the rock density contrasts caused by geological features on both regional (Arabian Sea basin) and local scales (Makran Trench). This is supported by an integrated analysis of the datasets indicating that differences in the gravity fields are caused by the variations in the geological basement structure and evolution in tectonic formation of the Makran, which is mirrored on the topographical maps. Gravity anomalies correlate with the boundaries of the Arabian Sea basin, which is characterized by a lower value on its topographical depths (Owen Fracture Zone, Makran Trench, the areas east of Somalia) and higher values in the mountain areas (Zagros, Oman). Prominent gravity lineaments may delineate faults and local basins.

The across-axis bathymetric profiles are drawn perpendicular to the stretching direction of the Makran Trench and across the segment of a 300-km distance (i.e. 150 km from the center of the cross--section). Total segment width is about 266 km (stretching from 61.3°E to 63.7°E). The error bars (vertical grey lines perpendicular to the median red-color line, Fig. 6A) are calculated as a statistical representation of the variability of the bathymetric and topographic data. They are plotted on a graph (Fig. 6A) to graphically indicate error or uncertainties in a GEBCO grid. The distance between the foot of the trench is reaching –3,487 m depth bounding the margins of the axial valley of the Makran Trench seafloor. The maximum and minimum detected depths of the Makran Trench are –3,487 m (the deepest part of the axial valley) and 43 m (the highest part of the coastal flank in the selected segment, Fig. 6A). A comparison is made between the parameters depicting the Makran Trench geomorphology, across-axis bathymetry, axial width (300 km), geological and geophysical framework (marine free-air gravity, geoid undulations), tectonics and sediment thickness. The steep northern slope of the trench is located on a Makran accretionary wedge (prism). Hence, its geomorphology is largely influenced by the structure, lithology, facies and age of the building rocks, as well as tectonic lineaments and processes, including faults, out-of-sequence dislocations, and thrusts. The southern, gently dipping slope is a fragment of a rather flat seafloor. The elevation behind the trench indicates the Murray Ridge.

The analysis of the bathymetric data distribution frequency (Fig. 7), normalized over 300-km width statistical windows for the Makran Trench, comprises data for the 13 cross-section profiles drawn as individual trench segments, averaged and binned into sections with flanks on each of the 150 m from the trench axis (Fig. 6). The analysis of trench bathymetry revealed following statistical results (Fig. 7). The most frequent depth (448 values) are detected at depths –3,250 to –3,500 m followed by values of –3,000 to –3,250 m (225 samples) and an interval of –2,750 to –3,000 m (201 sample). The gently declining continental slope of the coastal elevations correlates with the gradually decreasing frequency of depth, as shown in Figure 7: several equally distributed bins with sample values of 124 samples (–2,500 to –2,750 m), 96 samples (–2,250 to –2,500 m), 86 (–2,000 to –2,250 m), respectively. The second slight increase in topographical values (104 samples for the range of –1,750 to 2,000 m) indicates submarine elevations near the coastal line followed by a gradual decrease in values from 63 to 28 samples on the shelf area in total covering shelf area with bathymetry from –1,750 to –250 m. A higher peak can be seen for the near-coastal zone (205 sample points for the interval 0–250 m) followed by the terrain areas. At the deepest values exceeding –3,500 m there are only 14 samples detected: 13 samples for the range –3,500 to –3,750 m and one sample for the deepest zone having the lowest frequency typical for the deepest areas due to its local geological context and the impact of tectonic plate movements.

DISCUSSION

The deepest oceanic trenches are located in the western Pacific Ocean, followed by the eastern Pacific Ocean and Indian Ocean. Therefore, the Makran Trench is much shallower and has an irregular geomorphic shape compared to other oceanic trenches. The greatest trench depths of 10–11 km are detected in the Mariana and Tonga-Kermadec

trenches, while the Makran Trench does not exceed –3,487 m according to this study based on GEBCO dataset. The specific irregular shape form of the trench is caused by the dense lithosphere of the Arabian Plate subducting beneath the less-dense lithosphere of the Eurasian plate, which creates a trench at the convergent plate boundaries. In general, oceanic trenches vary according to their geomorphological type (U, V, asymmetric, symmetric) with characteristic steepness such as 'strong', 'very strong', 'extreme', 'steep', 'very steep', and the Makran Trench has a 'strong' slope clearly asymmetric on the continental slope and rather flat valley on the oceanward side. The valley slopes of the trenches can be classified as follows: very high, high, moderate, low based on the degree of curvature. Using this classification, the Makran Trench has a 'high' slope steepness on the continental slope of Pakistan, while it has a 'low' slope steepness on the oceanward side.

Topographical, gravity, geoid and geological data are related to the different rock properties in the subsurface. This results in the coinciding attribute contrasts clearly visible in the maps, a phenomenon which forms the basis for the joint spatial analysis and interpretation of the thematic data. This study examined the relationships between the topographical structure and submarine geomorphology, sediment thickness, geophysical anomaly fields, geological settings and tectonic lineament stretching of the Arabian Sea region, seafloor spreading rate, Carlsberg Ridge morphology and Makran Trench depths by GMT. Compared to other deep-sea trenches, the Makran Trench differs in its geomorphology. For instance, the Kuril-Kamchatka Trench has a cascade-shaped form. Variations in its geomorphology show (Lemenkova 2019e, 2020d) that the southern part reaches maximal depths of –8,200 m, while northern reaches those of –7,800 m. The Palau Trench is notable for its irregular V-shaped left-sided trench. Its bathymetric profiles have a very sharp yet irregular V-shape except for its northern portion (Lemenkova 2019f). The Mariana Trench is markedly symmetric, with a V-shaped bottom profile of large width. The dominating grades are steep (7–9°) and flat bottomed (Lemenkova 2019a). The Peru-Chile Trench is 4,500 km long, reaching depths of 7–8 km below sea level (Lemenkova 2019d). Because ocean trenches result from tectonic activity arising from the movement of the Earth's lithosphere, the shapes of the ocean trenches are diverse due to the regional geological settings, rock mineral composition, and erosion.

A geospatial analysis of the multi-source dataset using GMT presents a data-driven modelling technique with a scripting approach. Such an approach is useful when a correlation between the geomorphic data and complex geophysical processes underlying a phenomenon of the oceanic trench formation are only partially known, and would necessitate the mapping of a series of multi-source input raster data. The automatization of cartographic techniques is important, and a constantly developing challenge in geoinformatics (Freeman 1988, Ruas 1995, Hangouet 1998, Gauger et al. 2007, Schenke & Lemenkova 2008, Lemenkova 2018, 2019h, 2019i). Within the suite of data-driven GMT, a scripting approach is useful for automatic data processing from various sources (tectonics, sedimentology, geology, geophysics, geomorphology (geomorphometry) and topography). GMT presents a scripting template for the rapid processing of diverse datasets: set up of cartographic projections, legends, color tables, cartographic grid lines and ticks, choosing elements visualized on a map. The scripting templates of GMT facilitate the speed and increase the precision of mapping through automatization.

Automatization in GIS technically aims at increasing the speed of the technical processes, together with securing the reliability of the resulting output through the machine-based data analysis, free of human subjectivity during manual cartographic routine. Rapid and automated processing of various datasets by GMT enables different levels of cartographic abstraction, visual representation, data transformation (projections) and scale (both in terms of geographic scale and cartographic generalization of the level of details). Automatization in GIS mapping through scripting based GMT techniques enables us to speed up processing grids and focus on geophysical analysis. Compared to existing GIS, e.g. ArcGIS (Suetova et al. 2005, Lemenkova 2011, Lemenkova et al. 2012, Klaučo et al. 2013a, 2013b, 2014, 2017); the advantage of GMT is that it is able to process large

datasets in a rapid yet effective way rather than creating layouts for each map through the traditional GUI GIS interface.

CONCLUSIONS

This study aimed at analyzing the geomorphology of the Makran Trench in the context of the regional settings of the north Arabian Sea. Data integration is needed for the comparative analysis of the geomorphic structure of the Makran Trench (bathymetry, geology, geomorphology, geophysics). To achieve this purpose, GMT based cartographic methods were applied to high-resolution datasets, evaluated, modelled and visualized for the study area. Scripting techniques of GMT were executed to perform machine-based mapping with several GMT modules: 1) psbasemap pscoast, 2) grdcontour, 3) psxy, 4) psmeca, and 5) pslegend being the most important ones. The results showed the impact on the topography of the Makran Trench of geological, tectonic and geophysical regional settings. There are significant connections between the geomorphological modelling, tectonic and geological structure of the Makran Trench in the Arabian Sea. Therefore, the geomorphological features are a sensitive indicator for the interpretation of the submarine geological structures of the trench in the context of the geological and geophysical settings of the oceanic basin, where the availability of direct research is strictly limited by remote sensing approaches. Because the area of the study is tectonically active, with a system of ridges and fracture zones, it separates the Arabian Sea into morphologically distinct basins. Therefore, this study presented the analysis of the relationships between the topographic structure of the Makran Trench and regional settings of the Arabian Sea: geomorphology, sediment thickness, geophysical anomaly fields, geology and tectonic lineaments.

The analysis has shown that there is a correlation between the geological (tectonic) structure, asymmetric terrain forms and geophysical anomaly fields. For example, the gravity data indicate a crustal structure: the gravity anomaly is generated by the bending of the lithosphere into the Makran subduction zone and density variations in the mantle which is reflected in the gravity maps. The marine free-air gravity correlates with the lineaments of the geomorphic structures. The bathymetric analysis of the trench revealed the most frequent depth (448 samples) at –3,250 to –3,500 m, following by intervals: –3,000 to –3,250 m, –2,750 to –3,000 m. Declining continental slope of the coastal elevations correlate with gradually decreasing depths, as equally distributed bins: 124 samples (–2,500 to –2,750 m), 96 (–2,250 to –2,500 m), 86 (–2,000 to –2,250 m). The Makran Trench is an asymmetric form with a 'high' slope steepness on the continental slope of Pakistan, and a 'low' steepness with a rather flat valley on the oceanward side.

The multi-source data integration demonstrated is important for the seafloor mapping and geomorphological analysis of oceanic trenches hidden for direct observations. The machine learning methods of GMT and cartographic modeling provide possibilities for the efficient visualization and mapping the morphology of oceanic trenches. The comparison of the geomorphic models with gravity anomalies, tectonic lineation, geological structures and topographical variations of depths gives more detail to studies of the seafloor in the basin of the Arabian Sea. Further research might be based on expanded geodatasets (e.g. magnetic anomalies, stratigraphic columns) to understand the extent to which the effects of geology and tectonics have an impact on the geomorphology of the trench using modelling in other segments of the Makran Trench.

The effective GMT-based cartographic visualization demonstrating the models of the terrain features facilitates the reading of the elements of the geological structure, either directly or by a comparative analysis of the thematic maps and auxiliary cross-sections and enables more insightful observations about the local relations between geology and geomorphology. Another advantage of GMT consists in its high level of scientific graphical plotting, together with aesthetic geometric representation of the elements of maps (lines, polygons, symbols). Traditional mapping, using a user interface based on GIS, is less effective in term of precision and speed of mapping, compared to the machine-based cartographic visualization of GMT scripting toolset. As a result, GMT-based mapping is more appropriate than proprietary GIS maps.

As demonstrated in the presented paper, the GMT approach gives better results when dealing with large heterogeneous data for a complex analysis of various datasets (geology, tectonics, geophysics, topography, geomorphological modelling by cross-section profiles) than traditional GIS techniques that require lots of manual work. Second, the GMT is an open source toolset which presents a certain advantage over commercial GIS. Finally, GMT has embedded specific modules for plotting geophysical elements (focal mechanisms of so called 'beach balls' representing seismic settings, as plotted in Figure 2). Therefore, the traditional GIS cannot be seen as a complete equivalent to the GMT. The scripting nature of GMT means that the reproduction of spatial and temporal context is automated using prepared templates applied for various datasets which facilitates and automates the process of cartographic mapping.

Funding: China Scholarship Council (CSC), State Oceanic Administration (SOA), Marine Scholarship of China, Grant No. 2016SOA002, China. I would like to cordially thank the four anonymous reviewers and the editor for their helpful comments on the manuscript, all of which improved both the text and the maps.

REFERENCES

Abedi M. & Bahroudi A., 2016. A geophysical potential field study to image the Makran subduction zone in SE of Iran. *Tectonophysics*, 688, 119–134.

Agard P., Omrani J., Jolivet L., Whitechurch H., Vrielynck B., Spakman W., Monié P., Meyer B. & Wortel R., 2011. Zagros orogeny: a subduction-dominated process. *Geological Magazine*, 148, 5–6, 692–725. https://doi.org/10.1017/S001675681100046X.

Alavi M., 1980. Tectonostratigraphic evolution of the Zagrosides of Iran. *Geology*, 8, 144–149.

Al-Lazki A.I., Al-Damegh K.S., El-Hadidy S.Y., Ghods A. & Tatar M., 2014. Pn-velocity structure beneath Arabia-Eurasia Zagros collision and Makran subduction zones. [in:] Rollinson H.R., Searle M.P., Abbasi I.A., Al-Lazki A.I. &d Al-Kindi M.H., *Tectonic Evolution of the Oman Mountains*, Geological Society, Special Publication, 392, Geological Society of London, 45–60. https://doi.org/10.1144/SP392.3.

Awad M.B., El-Gendy A., El-Ghamri M.A., Hussein S.A. & Hamouda A.Z., 2001. Neotectonics of the Gulf of Aqaba, Red Sea, interpreted from gravity and deep seismic data. [in:] *Proceeding of the 2nd International Symposium on Geophysics (ISG-2), 19-20 February, 2001, Tanta University, Egypt*, 13–26.

Berberian F., Muir I.D., Pankhurst R.J. & Berberian M., 1982. Late cretaceous and early Miocene Andean-type plutonic activity in northern Makran and Central Iran. *Journal of the Geological Society*, 139, 5, 605–614. https://doi.org/10.1144/gsjgs.139.5.0605.

Bhattacharya G.C., Chaubey A.K., Murty G.P.S., Srinivas K., Sarma K.V.L.N.S., Subrahmanyam V. & Krishna K.S., 1994. Evidence for seafloor spreading in the Laxmi Basin, northeastern Arabian Sea. *Earth and Planetary Science Letters*, 125, 211–220. https://doi.org/10.1016/0012-821X(94)90216-X.

Bosworth W., Huchon P. & McClay K., 2005. The Red Sea and Gulf of Aden Basins. *Journal of African Earth Sciences*, 43, 1–3, 334–378. https://doi.org/10.1016/j.jafrearsci.2005.07.020.

Bourget J., Zaragosi S., Ellouz-Zimmermann S., Ducassou E., Prins M.A., Garlan T., Lanfumey V., Schneider J.-L., Rouillard P. & Giraudeau J., 2010. Highstand vs. lowstand turbidite system growth in the Makran active margin: Imprints of high-frequency external controls on sediment delivery mechanisms to deep water systems. *Marine Geology*, 274, 1–4, 187–208. https://doi.org/10.1016/j.margeo.2010.04.005.

Burg J.P., 2018. Geology of the onshore Makran accretionary wedge: Synthesis and tectonic interpretation. *Earth-Science Reviews*, 185, 1210–1231. https://doi.org/10.1016/j.earscirev.2018.09.011.

Burg J.-P., Dolati A., Bernoulli D. & Smit J., 2013. Structural style of the Makran Tertiary accretionary complex in SE-Iran. [in:] Al Hosani K., Roure F., Ellison R. & Lokier S. (eds.), *Lithosphere Dynamics and Sedimentary Basins: The Arabian Plate and Analogues*, Springer Verlag, Heidelberg, 239–259.

Delaloye M. & Desmons J., 1980. Ophiolites and melange terranes in Iran: a geochronological study and its paleotectonic implications. *Tectonophysics*, 68, 1, 83–111. https://doi.org/10.1016/0040-1951(80)90009-8.

Ekström G., Nettles M. & Dziewonski A.M., 2012. The global CMT project 2004-2010: Centroid-moment tensors for 13,017 earthquakes. *Physics of the Earth and Planetary Interiors*, 200–201, 1–9.

Ellouz-Zimmermann N., Deville E., Müller C., Lallemant S., Subhani A.B. & Tabreez A.R., 2007. Impact of sedimentation on convergent margin tectonics: example of the Makran Accretionary Prism (Pakistan). [in:] Lacombe O., Lavé J., Roure F. & Vergés J. (eds.), *Thrust Belts and Foreland Basins: From Fold Kinematics to Hydrocarbon Systems*, Springer Verlag, Berlin, 327–350. https://doi.org/10.1007/978-3-540-69426-7_17.

Farah A., Lawrence R.D. & Dejong K.A., 1984. An overview of the tectonics of Pakistan. [in:] Haq B.U. & Milliman J.D. (eds.), *Marine Geology and Oceanography of Arabian Sea and Coastal Pakistan*, Van Nostrand Reinhold/Scientific and Academic Editions, 161–176.

Freeman H., 1988. An expert system for the automatic placement of names on a geographic map. *Information Sciences*, 45, 367–378.

Gauger S., Kuhn G., Gohl K., Feigl T., Lemenkova P. & Hillenbrand C., 2007. Swath-bathymetric mapping. *Reports on Polar and Marine Research*, 557, 38–45.

Gaedicke C., Schlüter H.-U., Roeser H.A., Prexl A., Schreckenberger B., Meyer H., Reichert C., Clift P. & Amjad S., 2002. Origin of the northern Indus Fan and Murray Ridge, Northern Arabian Sea: interpretation from seismic and magnetic imaging. *Tectonophysics*, 355, 1–4, 127–143. https://doi.org/10.1016/S0040-1951(02)00137-3.

Glennie K.W., Hughes Clarke M.W., Boeuf M.G.A., Pilaar W.F.H. & Reinhardt B.M., 1990. Inter-relationship of Makran-Oman Mountains belts of convergence. [in:] Robertson A.H.F., Searle M.P. & Ries A.C. (eds.), *The Geology and Tectonics of the Oman Region*, Geological Society, London, Special Publications, 49, Geological Society of London, 773–786. https://doi.org/10.1144/GSL.SP.1992.049.01.47.

Goodenough K.M., Thomas R.J., Styles M.T., Schofield D.I. & MacLeod C.J., 2014. Records of ocean growth and destruction in the Oman–UAE Ophiolite. *Elements*, 10, 2, 109–114. https://doi.org/10.2113/gselements.10.2.109.

Grando G. & McClay K., 2007. Morphotectonics domains and structural styles in the Makran accretionary prism, offshore Iran. *Sedimentary Geology*, 196, 1–4, 157–179.

Haghipour N., Burg J.-P., Ivy-Ochs S., Hadjas I., Kubuk P.W. & Christl M., 2015. Correlation of fluvial terraces and temporal steady-state incision on the onshore Makran accretionary wedge in southeastern Iran: insight from channel profiles and 10Be exposure dating of strath terraces. *Geological Society of America Bulletin*, 127, 3–4, 560–583. https://doi.org/10.1130/B31048.1.

Hosseini-Barzi M. & Talbot C.J., 2003. A tectonic pulse in the Makran accretionary prism recorded in Iranian coastal sediments. *Journal of the Geological Society*, 160 (6), 903–910. https://doi.org/10.1144/0016-764903-005.

Hangouet J.F., 1998. *Approches et méthodes pour l'automatisation de la généralisation cartographique; application en bord de ville*. Université de Marne La Vallée, Paris [Ph.D. thesis].

Harms J.C., Cappel H.N. & Francis D.C., 1984. The Makran coast of Pakistan: its stratigraphy and hydrocarbon potential. [in:] Haq B.U. & Milliman J.D. (eds.), *Marine Geology and Oceanography of Arabian Sea and Coastal Pakistan*, Van Nostrand Reinhold/Scientific and Academic Editions, 3–27.

Hinze W., Von Frese R. & Saad A., 2013. *Gravity and Magnetic Exploration: Principles, Practices, and Applications*. Cambridge University Press, Cambridge. https://doi.org/10.1017/CBO9780511843129.

Hunziker D., Burg J.P., Bouilhol P. & von Quadt A., 2015. Jurassic rifting at the Eurasian Tethys margin: geochemical and geochronological constraints from granitoids of North Makran, southeastern Iran. *Tectonics*, 34, 3, 571–593. https://doi.org/10.1002/2014TC003768.

Hussain J., Butt K.A. & Pervaiz K., 2002. Makran coast: a potential seismic risk belt. *Geological Bulletin (University of Peshawar)*, 35, 43–56.

Jacob K.H. & Quittmeyer R.C., 1979. The Makran Region of Pakistan and Iran: Trench-arc system with active plate subduction. [in:] Farah A. & Dejong K.A. (eds.), *Geodynamics of Pakistan*, Geological Survey of Pakistan, Quetta, 305–317.

Kananian A., Juteau T., Bellon H., Darvishzadeh A., Sabzehi M., Whitechurch H. & Ricou L.-E., 2001. The ophiolite massif of Kahnuj (western Makran, southern Iran): new geological and geochronological data. *Comptes Rendus de l'Académie des Sciences – Series IIA – Earth and Planetary Science*, 332, 9, 543–552.

Klaučo M., Gregorová B., Stankov U., Marković V. & Lemenkova P., 2013a. Determination of ecological significance based on geostatistical assessment: a case study from the Slovak Natura 2000 protected area. *Central European Journal of Geosciences*, 5, 1, 28–42. https://doi.org/10.2478/s13533-012-0120-0.

Klaučo M., Gregorová B., Stankov U., Marković V. & Lemenkova P., 2013b. Interpretation of Landscape Values, Typology and Quality Using Methods of Spatial Metrics for Ecological Planning. [in:] *54th International Conference Environmental & Climate Technologies*. https://doi.org/10.13140/RG.2.2.23026.96963.

Klaučo M., Gregorová B., Stankov U., Marković V. & Lemenkova P., 2014. Landscape metrics as indicator for ecological significance: assessment of Sitno Natura 2000 sites, Slovakia. [in:] *Ecology and Environmental Protection. Proceedings of the International Conference, Minsk, March 19–20, 2014*, 85–90.

Klaučo M., Gregorová B., Stankov U., Marković V. & Lemenkova P., 2017. Land planning as a support for sustainable development based on tourism: A case study of Slovak Rural Region. *Environmental Engineering and Management Journal*, 2, 16, 449–458. https://doi.org/10.30638/eemj.2017.045.

Kopp C., Fruehn J., Flueh E.R., Reichert C., Kukowski N., Bialas J. & Klaeschen D., 2000. Structure of the Makran subduction zone from wide-angle and reflection seismic data. *Tectonophysics*, 329, 1–4, 171–191. https://doi.org/10.1016/S0040-1951(00)00195-5.

Kuhn G., Hass C., Kober M., Petitat M., Feigl T., Hillenbrand C.D., Kruger S., Forwick M., Gauger S. & Lemenkova P., 2006. The response of quaternary climatic cycles in the South-East Pacific: development of the opal belt and dynamics behavior of the West Antarctic ice sheet. [in:] Gohl K. (ed.), *Expeditionsprogramm Nr. 75 ANT XXIII/4*. https://doi.org/10.13140/RG.2.2.11468.87687.

Laane J.L. & Chen W.-P., 1989. The Makran earthquake of 1983 April 18: a possible analogue to the Puget Sound earthquake of 1965? *Geophysical Journal International*, 98, 1, 1–9. https://doi.org/10.1111/j.1365-246X.1989.tb05509.x.

Lemenkova P., 2011. *Seagrass Mapping and Monitoring Along the Coasts of Crete, Greece*. University of Twente, Netherlands [M.Sc. thesis].

Lemenkova P., 2018. R scripting libraries for comparative analysis of the correlation methods to identify factors affecting Mariana Trench formation. *Journal of Marine Technology and Environment*, 2, 35–42. https://doi.org/10.6084/m9.figshare.7434167.

Lemenkova P., 2019a. Statistical Analysis of the Mariana Trench Geomorphology Using R Programming Language. *Geodesy and Cartography*, 45, 2, 57–84. https://doi.org/10.3846/gac.2019.3785.

Lemenkova P., 2019b. Topographic surface modelling using raster grid datasets by GMT: example of the Kuril-Kamchatka Trench, Pacific Ocean. *Reports on Geodesy and Geoinformatics*, 108, 9–22. https://doi.org/10.2478/rgg-2019-0008.

Lemenkova P., 2019c. GMT Based Comparative Analysis and Geomorphological Mapping of the Kermadec and Tonga Trenches, Southwest Pacific Ocean. *Geographia Technica*, 14, 2, 39–48. https://doi.org/10.21163/GT_2019.142.04.

Lemenkova P., 2019d. Geomorphological modelling and mapping of the Peru-Chile Trench by GMT. *Polish Cartographical Review*, 51, 4, 181–194. https://doi.org/10.2478/pcr-2019-0015.

Lemenkova P., 2019e. AWK and GNU Octave Programming Languages Integrated with Generic Mapping Tools for Geomorphological Analysis. *GeoScience Engineering*, 65, 4, 1–22. https://doi.org/10.35180/gse-2019-0020.

Lemenkova P., 2019f. Automatic Data Processing for Visualising Yap and Palau Trenches by Generic Mapping Tools. *Cartographic Letters*, 27, 2, 72–89. https://doi.org/10.6084/m9.figshare.11544048.

Lemenkova P., 2019g. Geophysical Modelling of the Middle America Trench using GMT. *Annals of Valahia University of Targoviste. Geographical Series*, 19, 2, 73–94. https://doi.org/10.6084/m9.figshare.12005148.

Lemenkova P., 2019h. An Empirical Study of R Applications for Data Analysis in Marine Geology. *Marine Science and Technology Bulletin*, 8, 1, 1–9. https://doi.org/10.33714/masteb.486678.

Lemenkova P., 2019i. Testing Linear Regressions by StatsModel Library of Python for Oceanological Data Interpretation. *Aquatic Sciences and Engineering*, 34, 51–60. https://doi.org/10.26650/ASE2019547010.

Lemenkova P., 2020a. Visualization of the geophysical settings in the Philippine Sea margins by means of GMT and ISC data. *Central European Journal of Geography and Sustainable Development*, 2, 1, 5–15. https://doi.org/10.6084/m9.figshare.12044799.

Lemenkova P., 2020b. Variations in the bathymetry and bottom morphology of the Izu-Bonin Trench modelled by GMT. *Bulletin of Geography. Physical Geography Series*, 18, 1, 41–60. https://doi.org/10.2478/bgeo-2020-0004.

Lemenkova P., 2020c. GMT Based Comparative Geomorphological Analysis of the Vityaz and Vanuatu Trenches, Fiji Basin. *Geodetski List*, 74, 1, 19–39. https://doi.org/10.6084/m9.figshare.12249773.

Lemenkova P., 2020d. GMT-based geological mapping and assessment of the bathymetric variations of the Kuril-Kamchatka Trench, Pacific Ocean. *Natural and Engineering Sciences*, 5, 1, 1–17. https://doi.org/10.28978/nesciences.691708.

Lemenkova P., Promper C. & Glade T., 2012. Economic Assessment of Landslide Risk for the Waidhofen a.d. Ybbs Region, Alpine Foreland, Lower Austria. [in:] Eberhardt E., Froese C., Turner A.K. & Leroueil S. (eds.), *Landslides and Engineered Slopes: Protecting Society Through Improved Understanding: Proceedings of the 11th International and 2nd North American Symposium on Landslides and Engineered Slopes, Banff, Canada, 3-8 June 2012*, vol. 1, CRC Press, Leiden, 279–285.

Lemoine F.G., Kenyon S.C., Factor J.K., Trimmer R.G., Pavlis N.K., Chinn D.S., Cox C.M., Klosko S.M., Luthcke S.B., Torrence M.H., Wang Y.M., Williamson R.G., Pavlis E.C., Rapp R.H. & Olson T.R., 1998. *NASA/TP-1998-206861: The Development of the Joint NASA GSFC and NIMA Geopotential Model EGM96*. NASA Goddard Space Flight Center, Greenbelt, Maryland, 20771 USA.

Linsser H., 1967. Investigation of tectonics by gravity detailing. *Geophysical Prospecting*, 15, 3, 480–515.

Lisitsyn A.P., 1974. *Osadkoobrazovaniyev okeanakh. Kolichestvennoye raspredeleniye osadochnogo materiala*. Nauka, Moskva [Лисицын А.П., 1974. *Осадкообразование в океанах. Количественное распределение осадочного материала*. Наука, Москва].

Mayer L., Jakobsson M., Allen G., Dorschel B., Falconer R., Ferrini V., Lamarche G., Snaith H. & Weatherall P., 2018. The Nippon Foundation – GEBCO Seabed 2030 Project: The Quest to See the World's Oceans Completely Mapped by 2030. *Geosciences*, 8, 2, 63. https://doi.org/10.3390/geosciences8020063.

McCall G.J.H., 1997. The geotectonic history of the Makran and adjacent areas of southern Iran. *Journal of Asian Earth Sciences*, 15, 6, 517–531. https://doi.org/10.1016/S0743-9547(97)00032-9.

Miles P.R., Munschy M. & Segoufin J., 1998. Structure and early evolution of the Arabian Sea and East Somali Basin. *Geophysical Journal International*, 134, 3, 876–888. https://doi.org/10.1046/j.1365-246x.1998.00625.x.

Minshull T.A., Edwards R.A. & Flueh E.R., 2015. Crustal structure of the Murray Ridge, northwest Indian Ocean, from wide-angle seismic data. *Geophysical Journal International*, 202, 1, 454–463. https://doi.org/10.1093/gji/ggv162.

Monahan D., 2004. GEBCO: the Second Century. D. Monahan, University of New Hampshire. *Hydro International*, 8, 9.

Motaghi K., Shabanian E. & Nozad-Khalil T., 2020. Deep structure of the western coast of the Makran subduction zone, SE Iran. *Tectonophysics*, 776, 228314. https://doi.org/10.1016/j.tecto.2019.228314.

Murton B.J. & Rona P.A., 2015. Carlsberg Ridge and Mid-Atlantic Ridge: Comparison of slow spreading centre analogues. *Deep-Sea Research II*, 121, 71–84.

Neprochnov Y.P., 1961. Sediment thickness in the basin of the Arabian Sea. *Reports of the Academy of Sciences USSR*, 139, 1.

Paul A., Hatzfeld D., Kaviani A., Tatar M. & Pequegnat C., 2010. Seismic imaging of the lithospheric structure of the Zagros mountain belt (Iran). [in:] Leturmy P. & Robin C. (eds.), *Tectonic and Stratigraphic Evolution of Zagros and Makran during the Mesozoic–Cenozoic*, Geological Society, Special Publications, 330, Geological Society of London, 5–18.

Pavlis N.K., Holmes S.A., Kenyon S.C. & Factor J.K., 2012. The development and evaluation of the Earth Gravitational Model 2008 (EGM2008). *Journal of Geophysical Research*, 117, B04406. https://doi.org/10.1029/2011JB008916.

Platt J.P., Leggett J.K., Young J., Raza H. & Alam S., 1985. Large-scale sediment underplating in the Makran accretionary prism. *Geology*, 13, 7, 507–511. https://doi.org/10.1130/0091-7613(1985)13<507:LSUITM>2.0.CO;2.

Purnachandra Rao V., 1986. Phosphorites from the Error Seamount, Northern Arabian Sea. *Marine Geology*, 71, 1–2, 177–186. https://doi.org/10.1016/0025-3227(86)90038-1.

Prins M.A., Postma G. & Weltje G.J., 2000. Controls on terrigenous sediment supply to the Arabian Sea during the late Quaternary: the Makran continental slope. *Marine Geology*, 169, 3–4, 351–371. https://doi.org/10.1016/S0025-3227(00)00087-6.

Rani V.S., Srivastava K., Srinagesh D. & Dimri V.P., 2011. Spatial and temporal variations of b-value and fractal analysis for the Makran region. *Marine Geodesy*, 34, 1, 77–82. https://doi.org/10.1080/01490419.2011.547804.

Regard V., Hatzfeld D., Molinaro M., Aubourg C., Bayer R., Bellier O., Yamini-Fard F., Peyret M. & Abbassi M., 2010. The transition between Makran subduction and the Zagros collision: recent advances in its structure and active deformation. [in:] Leturmy P. & Robin C. (eds.), *Tectonic and Stratigraphic Evolution of Zagros and Makran during the Mesozoic–Cenozoic*, Geological Society, London, Special Publications, 330, Geological Society of London, 43–64. https://doi.org/10.1144/SP330.4.

Rodriguez M., Chamot-Rooke N., Huchon P., Fournier M., Lallemant S., Delescluse M., Zaragosie S. & Mouchot N., 2014. Tectonics of the Dalrymple Trough and uplift of the Murray Ridge (NW Indian Ocean). *Tectonophysics*, 636, 1–17. https://doi.org/10.1016/j.tecto.2014.08.001.

Ruas A., 1995. Multiple paradigms for Automating Map Generalization: Geometry, Topology, Hierarchical Partitioning and Local Triangulation. *Proceedings of AutoCarto*, 12, Charlotte, NC: ACSM/ASPRS, 69–78.

Sandwell D.T., Müller R.D., Smith W.H.F., Garcia E. & Francis R., 2014. New global marine gravity model from CryoSat-2 and Jason-1 reveals buried tectonic structure. *Science* 346, 65–67. https://doi.org/10.1126/science.1258213.

Schlüter H.U., Prexl A., Gaedicke Ch., Roeser H., Reichert Ch., Meyer H. & von Daniels C., 2002. The Makran accretionary wedge: sediment thicknesses and ages and the origin of mud volcanoes. *Marine Geology*, 185, 3–4, 219–232. https://doi.org/10.1016/S0025-3227(02)00192-5.

Searle M.P., James N.P., Calon I.J. & Smewing J.D., 1983. Sedimentological and structural evolution of the Arabian continental margin in the Musandam Mountains and Dibba zone, United Arab Emirates. *Geological Society of America Bulletin*, 94, 12, 1381–1400. https://doi.org/10.1130/0016-7606(1983)94<1381:SASEOT>2.0.CO;2.

Selim E.I. & Aboud E., 2012. Determination of sedimentary cover and structural trends in the Central Sinai area using gravity and magnetic data analysis. *Journal of Asian Earth Sciences*, 43, 193–206. https://doi.org/10.1016/j.jseaes.2011.09.010.

Sengör A.M.C., Altiner D., Cin A., Ustaömer T. & Hsü K.J., 1988. The origin and assembly of the Tethyside orogenic collage at the expense of Gondwana land. [in:] Audley-Charles M.G. & Hallam A. (eds.), *Gondwana and Tethys*, Geological Society, London, Special Publications, 37, Geological Society of London, 119–181.

Smith W.H.F. & Sandwell D.T., 1997. Global seafloor topography from satellite altimetry and ship depth soundings. *Science*, 277, 1956–1962.

Smith G.L., McNeill L.C., Henstock T.J., Arraiz D. & Spiess V., 2014. Fluid generation and distribution in the highest sediment input accretionary margin, the Makran. *Earth and Planetary Science Letters*, 403, 1, 131–143. https://doi.org/10.1016/j.epsl.2014.06.030.

Schenke H.W. & Lemenkova P., 2008. Zur Frage der Meeresboden-Kartographie: Die Nutzung von AutoTrace Digitizer für die Vektorisierung der Bathymetrischen Daten in der Petschora-See. *Hydrographische Nachrichten*, 81, 16–21.

Stein C.A. & Cochran J.R., 1985. The transition between the Sheba Ridge and Owen Basin: rifting of old oceanic lithosphere. *Geophysical Journal Royal Astronomical Society*, 81, 1, 47–74.

Straume E.O., Gaina C., Medvedev S., Hochmuth K., Gohl K., Whittaker J.M., Abdul Fattah R., Doornenbal J.C. & Hopper J.R., 2019. GlobSed: Updated total sediment thickness in the world's oceans. *Geochemistry, Geophysics, Geosystems*, 20, 4, 1756–1772. https://doi.org/10.1029/2018GC008115.

Suetova I.A., Ushakova L.A. & Lemenkova P., 2005. Geoinformation mapping of the Barents and Pechora Seas. *Geography and Natural Resources*, 4, 138–142. https://doi.org/10.6084/m9.figshare.7435535.

Takin M., 1972. Iranian Geology and Continental Drift in the Middle East. *Nature*, 235, 147–150.

Vernant P., Nilforoushan F., Hatzfeld D., Abbassi M.R., Vigny C., Masson F., Nankali H., Martinod J., Ashtiani A., Bayer R., Tavakoli F. & Chéry J., 2004. Present-day crustal deformation and plate kinematics in the Middle East constrained by GPS measurements in Iran and northern Oman. *Geophysical Journal International*, 157, 1, 381–398. https://doi.org/10.1111/j.1365-246X.2004.02222.x.

White R.S. & Klitgord K., 1976. Sediment deformation and plate tectonics in the Gulf of Oman. *Earth and Planetary Science Letters*, 32, 2, 199–209. https://doi.org/10.1016/0012-821X(76)90059-5.

White R.S., 1982. Deformation of the Makran accretionary sediment prism in the Gulf of Oman (north-west Indian Ocean). [in:] Leggett J.K. (ed.), *Trench-Forearc Geology: Sedimentation and Tectonics on Modern and Ancient Active Plate Margins*, Geological Society, Special Publications, 10, 1, Geological Society of London, 357–372.

Wessel P. & Smith W.H.F., 1991. Free software helps map and display data. *EOS Transactions of the American Geophysical Union*, 72, 41, 441.

Wessel P. & Smith W.H.F., 2018. *The Generic Mapping Tools. Version 4.5.18 Technical Reference and Cookbook*. Computer software manual. U.S.A.

Wessel P., Smith W.H F., Scharroo R., Luis J.F. & Wobbe F., 2013. Generic mapping tools: Improved version released. *EOS Transactions of the American Geophysical Union*, 94, 45, 409– 410.

Wolff T., 1967. *Danish Expeditions on the Seven Seas*. Rhodos, Copenhagen.